A TRANSIENT PLASTICITY STUDY AND LOW CYCLE FATIGUE ANALYSIS OF THE SPACE STATION FREEDOM PHOTOVOLTAIC SOLAR ARRAY BLANKET

Sasan C. Armand and Mei-Hwa Liao
National Aeronautics and Space Administration
Lewis Research Center
Cleveland, Ohio 44135

and

Ronald W. Morris
Sverdrup Technology, Inc.
NASA Lewis Research Center Group
Cleveland, Ohio 44135

E-5321

ABSTRACT

The Space Station Freedom Photovoltaic solar array blanket assembly is comprised of several layers of materials having dissimilar elastic, thermal, and mechanical properties. The operating temperature of the solar array, which ranges from -75 to 60 °C, along with the material incompatibility of the blanket assembly components combine to cause an elastic-plastic stress in the weld points of the assembly. The weld points are secondary structures in nature, merely serving as electrical junctions for gathering the current. The thermal mechanical loading of the blanket assembly operating in low earth orbit continually changes throughout each 90 min orbit, which raises the possibility of fatigue induced failure. This paper describes the MSC/NASTRAN transient plasticity analysis and the low cycle fatigue calculations for the photovoltaic solar array blanket assembly.

INTRODUCTION

The solar cell assembly for the Space Station Freedom program is made up of several layers of materials having different coefficients of thermal expansion (CTE). Figure 1 shows a coupon of four solar cells. The layout of the copper interconnects which transmit current can be seen in this figure. Figure 2(a) depicts the Space Station Solar Array and an exploded view of the layers that make up a solar cell assembly. Figure 2(b) depicts the cross section of the blanket assembly and the solar cell assembly. Figure 3 depicts the cutaway detail of the solar cell assembly at the junction holes. As can be seen in these figures, the silver is vacuum plated onto the silicon, then the copper interconnect is welded onto the silver. The silver grids gather electrical current which in turn is transferred to the copper interconnect at the welded junction point.

The primary loading of the solar cell assembly is thermal loading induced by temperature changes encountered in low earth orbit. Figure 4 depicts a typical operating temperature profile for the solar arrays. At the sun portion of the orbit, the operating temperature of the cell assembly reaches a steady state temperature of 60 °C. The eclipse portion of the orbit produces a minimum temperature of -75 °C. Since the coefficients of thermal expansion of the

cell assembly layers that are bonded together (specifically silicon, silver, and copper) are different, the induced thermal stresses will cause a plastic deformation. Because the thermal loading of the cell assembly is cyclic in nature, fatigue failure could occur. Currently, samples of the solar cell assembly are undergoing a thermal cycling test which has already exceeded the space station requirement of 15 years or 87 500 cycles. The temperature range for the thermal cycling chamber is -90 to 70 °C per reference 5, which is more severe than the operating temperature range of the cell assembly. The thermal loading for the analysis in this paper uses the thermal cycling test temperature range.

NASA Lewis Research Center and Lockheed have developed a method under the Photovoltaic Array Environment Protection (PAEP) contract, NAS3-25079 to optimize the strength of the weld by varying parameters such as the pressure posed by the welding electrodes during welding, duration of welding, and the amount of current going through the electrodes (ref. 6). The analysis performed in this paper assumes a perfectly welded joint with no nonuniformity present.

FINITE ELEMENT STRUCTURAL ANALYSIS

This section describes the finite element models, the MSC/NASTRAN runs, and the objective of each model and run.

Overall Modeling Strategy

In order to keep the size of the finite element models down to a minimum, simplifying assumptions about the structure of the solar cells were made. The only portions of the cells modeled were the silicon cell itself, the copper interconnects, and the welds that bond the interconnects to the cell. The very first finite element model of the blanket assembly included all structural elements and layers of the assembly, but later on it was determined by analysis that some portions of the blanket assembly such as adhesives, glass covers, and layers of Kapton film are not structurally significant. Therefore, the nonsignificant structural elements of the blanket assembly were omitted from all models. In addition, the interconnects that run between individual cells have enough curvature in them that they will not be pulled taut at low temperatures and thus can be neglected also.

The points where the interconnects are welded to the silicon cell are best modeled with three layers of solid elements; one for the silicon cell, one for the weld interface, and one for the copper interconnect. The greatest strains occur in the interconnect near the weld points, so this area was modeled with solid elements also. All other parts of the cell and interconnect were modeled with plate elements in order to keep the size of the model down. Hexahedron (CHEXA) and quadrilateral (CQUAD4) elements were used wherever possible, including all areas where strains are high. Pentahedron (CPENTA) and triangular (CTRIA3) elements are used only where required by the geometry of the structure or for mesh transition. Rigid bar (RBAR) elements were used for transition from solid to plate elements.

Symmetry was used to reduce the size of the models whenever possible. Standard symmetry boundary conditions were applied to all grids on a plane of symmetry. An appropriate point in each model was constrained in order to prevent rigid body motion. The individual models will be described later.

There are several materials mixed together in the weld footprint. Silver, copper, silicon, titanium, pladdium are all present. The mixture percentages of all of these materials are very small when compared with the amount of copper (ref. 7). Therefore, the weld was assumed to be pure copper in the finite element analyses. Similar welds have been metallurgically analyzed in reference 7 which substantiate the basis of this assumption.

Static and Nonlinear Elastic-Plastic Analyses

The first MSC/NASTRAN runs were static analysis of the entire solar cell. One was conducted at a temperature of -90 °C and one at 70 °C. The symmetric geometry of the cells and the simplifying assumptions discussed previously allow the entire cell to be analyzed with a one-quarter model. That model is shown in figure 5. It consists of 1280 solid elements, 1143 plate elements, and 3335 grid points. Because the model is used only for static analysis, less care is observed in minimizing the size of the model.

The static analyses showed that the copper interconnect yields at both temperature extremes and thus must be subjected to nonlinear elastic-plastic analysis. It was also shown that, as one would expect, the highest strains occur in the longest copper interconnects (there are two per cell) near their weld points. This is due to the fact that the unit of CTE is inch per inch, and thus the longer copper interconnect should shrink or expand more than the shorter ones.

Two different mechanisms can cause strains in the interconnect when a thermal load is applied. One produces strains in and near the weld footprint due to having two materials with different CTE's welded together. The copper side of the weld is shrinking or expanding more than the silicon side of the weld. This mechanism acts during both the hot and cold portions of the thermal cycle.

The second mechanism is the interconnects pulling on the welds during the cold part of the cycle because they shrink more than the silicon cell does. The interconnects do not exert any force on the welds during the hot portion of the cycle because they will buckle with the slightest compressive load. This buckling phenomenon was confirmed by MSC/NASTRAN analysis as will be explained later on in this section.

Once it had been determined by static analysis which interconnect experienced the greatest strains, the nonlinear analysis could be limited to that interconnect. Symmetry allows the model to be limited to one-half of the interconnect and the silicon cell surrounding it. The model is shown in figure 6. The weld footprint is made up of two half circles and is shaded in the figure. The model consists of 198 solid elements, 276 plate elements, and 732 grid points. The model is more detailed in the weld area because the highest strains occur there. This half interconnect model was used for the analysis of

the cold portion of the thermal cycle because it reflects both strain mechanisms described above.

This analysis assumed that the interconnects would never be permanently deformed during their 15 year expected life. In reality, one would expect permanent plastic deformations to occur. This expectation was confirmed in the thermal cycling test program described earlier (ref. 5). These deformations would provide "slack" that would have to be pulled taut before strains would occur near the welds under cold temperatures. Therefore, the analysis described above can be considered to be a worst case analysis.

Because the strain mechanism acting during the hot part of the cycle acts only in the weld area, the high temperature nonlinear analysis can be limited to a model of one such area. Symmetry allows modeling of only one-quarter of the weld area. The model is shown in figure 7. It includes the weld footprint and a small radius of the interconnect and cell that surround it. The footprint is shaded in the figure. The model consists of 87 solid elements and 236 grid points.

In summary, two finite element runs were required to simulate the thermal cycles the cells would be subjected to: one for the hot side and one for the cold side. The cold side run used the model in figure 6 and a temperature load of -90 °C. The hot side run used the model in figure 7 and a temperature load of 70 °C. The reference temperature in both runs was 20 °C. The temperature extremes were chosen to match those used in the thermal cycling tests of the solar cells currently being conducted here at LeRC. Because the copper interconnects will undergo plastic deformation when subjected to these temperature extremes, the analysis method used was nonlinear elastic-plastic (MSC/NASTRAN solution 66).

Buckling and Transient Plasticity Analyses

To determine if permanent deformations would be caused by the thermal loading of the copper interconnect, a finite element model of the copper interconnect was isolated from the rest of the cell assembly model and subjected to two additional MSC/NASTRAN runs. Applicable boundary conditions (see Overall Modeling Strategy) and single point constraint forces obtained from the analysis of the one half interconnect model (fig. 6) were applied to this new interconnect model.

For the compressive loading portion of this analysis, solution sequence 99, which is capable of solving transient (time dependent) elastic-plastic problems, was used. Figure 8 depicts the first buckling mode of the copper interconnect and figure 9 depicts the Z-direction displacement of circled node in figure 8 as function of time. A fictitious transient time for this solution was used and was stretched to minimize any probable inertia effects. The reason for using solution sequence 99 for buckling analysis was to take advantage of the XYPA plotting module of MSC/NASTRAN. The XYPA plotting module provided plots of the instability of the copper interconnect as a function of the loading history.

A second MSC/NASTRAN analysis of the copper interconnect was made which used the tensile loads of the single point constraint forces taken from analysis of the one half interconnect model. For this run, solution sequence 66 of MSC/NASTRAN was used. The objective was to determine the effect of the tensile loads exerted on the copper interconnect. In general terms, this run analyzed the effect of plasticity on the copper interconnect and determined if the copper interconnect would apply any additional load on the weld points. To simulate loading of the copper interconnect, three subcases in solution sequence 66 were used. Subcase 1 used the maximum tensile loads of the single point constraint forces. In subcase 2, all forces were zeroed out. In subcase 3, the maximum tensile loads were reapplied. A detailed discussion of the results obtained from this run will be given later.

FATIGUE ANALYSIS

At completion of the structural analysis, a fatigue analysis was performed. Coffin (ref. 1) and Manson (ref. 2) have suggested the following empirical equation to determine the fatigue life:

$$e_t = D^{0.6} N_f^{-0.6} + 3.5 \frac{F_u}{E} N_f^{-0.12} \qquad (1)$$

where

e_t strain range
D ductility coefficient
F_u ultimate strength
E modulus of elasticity
N_f number of cycles to failure

As can be seen in this equation, calculating the fatigue behavior depends largely upon having an accurate ultimate strength (F_u) and ductility coefficient (D).

Equation (1) represents the strain range for a uniaxial specimen. The strains obtained from the finite element structural analysis are multiaxial and therefore must be combined to represent a one dimensional strain. Fuchs and Stevens (ref. 3) have suggested that the multiaxial plastic strains should be combined using equation (2):

$$e_t = \frac{1}{(1 + v)\sqrt{2}} \sqrt{\left(\Delta e_x - \Delta e_y\right)^2 + \left(\Delta e_y - \Delta e_z\right)^2 + \left(\Delta e_z - \Delta e_x\right)^2} \qquad (2)$$

Where v is Poisson's ratio, Δe_x, Δe_y, and Δe_z are the strains in the three principle directions and e_t is the total equivalent strain. Use of equation (2) was confirmed by Kaplan (ref. 4). Strains are used rather than stresses because the material in question yields.

The material property values used in equation (1) will change slightly as a function of temperature. However, Kaplan (ref. 4) has suggested that good

fatigue results can be obtained by using properties calculated at the mean operating temperature, which is room temperature (20 °C) for this analysis.

RESULTS

Nonlinear Elastic-Plastic and Fatigue Analysis

Strains calculated for the hot side of the cycle were subtracted from those calculated for the cold side of the cycle to obtain a total strain range for the cycle in X, Y, and Z. These strains were then input to equation (2) to obtain a single equivalent total strain. As expected, the highest total strain (which will produce the lowest cyclic life) occurs in the copper interconnect near (but not in) the weld footprint. The highest total strain was then input to equation (1) to obtain the lowest cyclic life. The alternating strain range used to determine the fatigue life in this paper is based on the first loading cycle. That is, it is assumed that the copper interconnect pulls on the weld joint during every cycle. It was thus determined that, in the worst case, fatigue failure would occur in 92 000 cycles (orbits of the space station), compared to the required life of 87 500 orbits. The 92 000 cycle fatigue life was calculated using the conservative portion of the material properties. When using the nonconservative material properties, the fatigue life is approximately 160 000 cycles.

Buckling and Transient Plasticity Analyses

The MSC/NASTRAN buckling analysis indicated high stresses and plastic strains in the copper interconnect. The plastic strains occur in two places: (1) the junction of the rectangular section to the circular section of the copper interconnect at the fillets and (2) the inside diameter of the interconnect. Although some portions of the copper interconnect deform beyond the elastic region and possess high residual strains, the overall contribution of this plastic strain to low cycle fatigue of the weld joint should be negligible. This is due to the fact that the high residual strains are not cyclic in nature, occurring only during the first loading cycle. Also, yielding and deformation of the copper interconnect under compressive loading should cause redistribution of the load in a uniform manner such that all regions of the weld joint can react to the cyclic compressive load more equally. Another important result of the buckling analysis was obtaining the first buckling mode of the copper interconnect Results of the thermal cycling test being performed presently at NASA Lewis have shown that the buckling of the copper interconnect indeed becomes permanent (ref. 5). This permanent buckling is quite noticeable during inspection of the test subjects at room temperature. The buckled copper interconnect superimposed on the undeformed figure has been shown in figure 8.

The MSC/NASTRAN runs for the tensile loading of the copper interconnect showed high stresses and plastic strains almost everywhere in the model. A plot of the displaced copper interconnect under the no loading condition has been shown in figure 10. As can be seen in this figure, the copper interconnect has deformed and stretched to the extent that during the second loading cycle and afterwards, the pulling on the weld joint from the copper interconnect due to decreases in temperature will be lessened. This lessened pulling causes the alternating strain range to be lessened also. Since one of the

two sources of loading and fatigue for the weld joint is the pull from the copper interconnect, it can be concluded that this lessened pull on the weld will increase the fatigue life beyond the 92 000 cycles calculated in the worst case analysis.

As the MSC/NASTRAN buckling and tensile loading analyses of the copper interconnect have shown, the interconnects are strained beyond the material yield point. A majority of the high strain areas were discovered to be at the edge of the weld in the copper interconnect. Prior to welding the copper interconnect to the silicon cell, it is customary to push the copper interconnect towards the silicon with the tip of a small eraser (ref. 6). This is to allow the operators to make a better weld. The result of this pushing action is a small dimple in the copper interconnect which can be seen with the naked eye. Combining the residual strains from this prewelding preparation (dimpling) and those from the thermal mechanical loading of the copper interconnect results in a failure of the copper interconnect at the weld joint. Specifically, the failure is the separation of portions of the copper interconnect from the silicon cell near the weld joint. Years of thermal cycling tests of various solar cell assemblies at NASA Lewis have shown that one of the failure modes of the solar cell assemblies is indeed the separation of the copper interconnect by itself (ref. 8). This is because the prewelding process (dimpling) cannot be exactly repeated. The residual strains caused by the dimpling may contribute to a longer fatigue life provided that the resulting alternating strain range is smaller.

CONCLUSIONS

A series of structural analyses have been performed in an attempt to predict the fatigue life of the solar cell in the Space Station Freedom photovoltaic array blanket.

A nonlinear elastic-plastic MSC/NASTRAN analysis followed by a fatigue calculation indicated a fatigue life of 92 000 to 160 000 cycles for the solar cell weld tabs. These results are for the worst case loading situation.

Additional analyses predict a permanent buckling phenomenon in the copper interconnect after the first loading cycle. This should reduce or eliminate the pulling of the copper interconnect on the joint where it is welded to the silicon solar cell.

It is therefore concluded that the actual fatigue life of the solar array blanket assembly should be significantly higher than the calculated 92 000 cycles, and thus the program requirement of 87 500 cycles (orbits) will be met.

Another important conclusion that can be drawn from the overall analysis is that, the strain results obtained from the MSC/NASTRAN nonlinear module are accurate to use for low-cycle fatigue analysis, since both thermal cycle testing of solar cells (ref. 5) and analysis have shown higher fatigue life than the minimum program requirement of 87 500 cycles.

REFERENCES

1. Coffin, L.F., Jr.: Design Aspects of High Temperature Fatigue With Particular Reference to Thermal Stresses. Trans. ASME, vol. 78, no. 3, Apr. 1956, pp. 527-532.

2. Manson, S.S.: Fatigue: A Complex Subject - Some Simple Approximations. Exper. Mech., vol. 5, no. 7, July 1965, pp. 193-226.

3. Fuchs, H.O.; and Stevens, R.I.: Metal Fatigue in Engineering. Wiley, 1980

4. Kaplan, A.: Fatigue Analysis of Solar Cell Welds. Tenth IEEE Photovoltaic Specialists Conference, IEEE, 1973, pp. 281-286.

5. Smith, B.K.: Thermal Cycle Testing of Space Station Freedom Solar Array Blanket Coupons. 1989 Space Photovoltaic Research and Technology Conference, NASA Lewis Research Center, Cleveland, OH, 1989.

6. Sater, B.L.: Personal Communication, NASA Lewis Research Center, Cleveland, OH (NASA Contract NAS3-25079, Photovoltaic Array Environment Protection).

7. Baroana, C.R., et al.: Evaluation of Electrode Shape and Nondestructive Evaluation Method for Welded Solar Cell Interconnects. Sixteenth IEEE Photovoltaic Specialists Conference, IEEE, 1982, pp. 90-95 (NASA TM-82966).

8. Hart, R.E.: Personal Communication, NASA Lewis Research Center, Cleveland, OH.

9. Schwartz, C.: Solar Array Program, Solar Thermal Analysis", Lockheed Monthly Program Status Review for Space Station Freedom Solar Power Module, Feb. 1989.

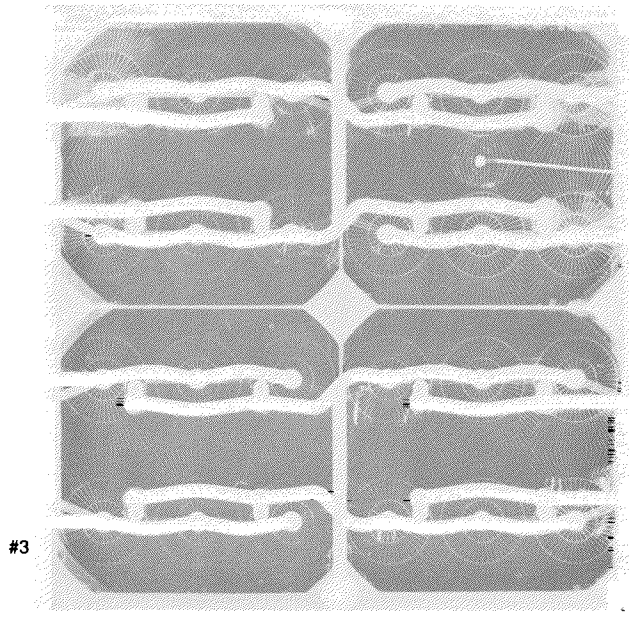

C-89-01830

Figure 1. - Coupon of four solar cells.

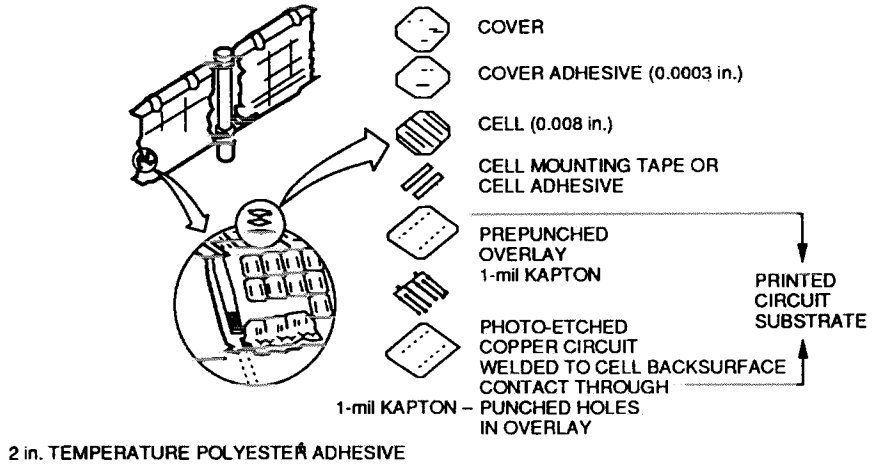

Figure 2a. - Exploded view of solar array.

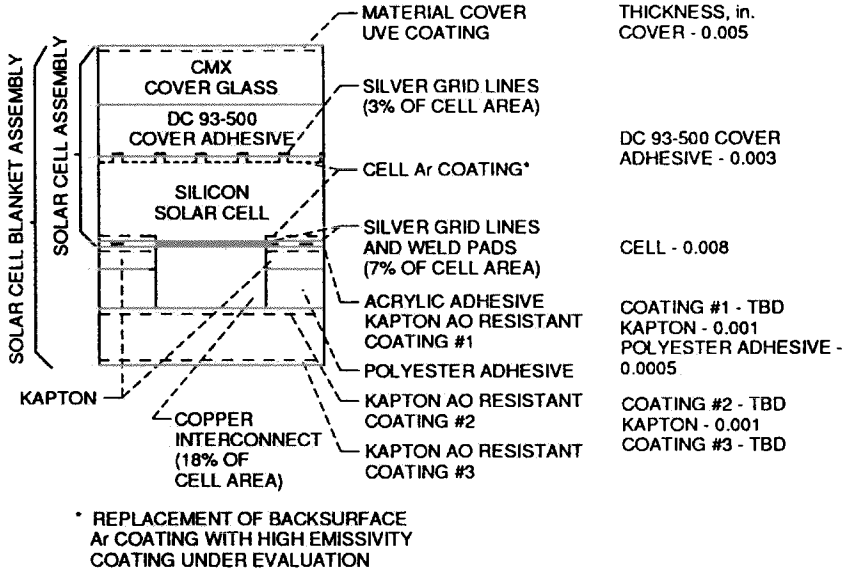

Figure 2b. - Cross section of solar cell blanket assembly.

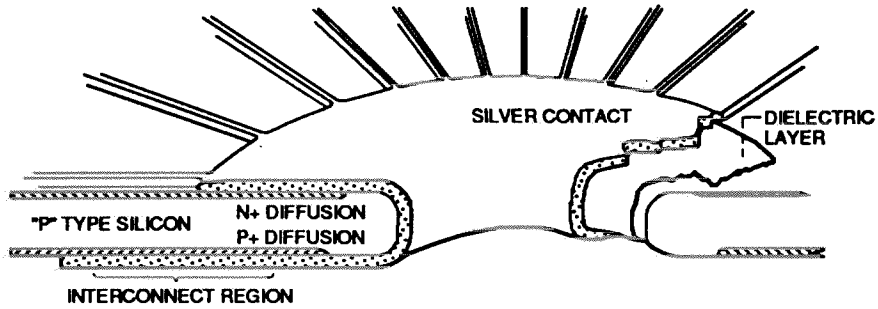

Figure 3. - Cutaway detail of space station solar cell.

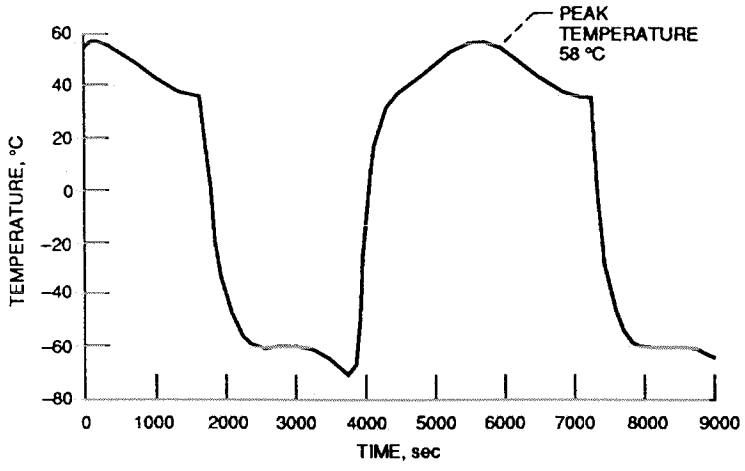

Figure 4. - Predicted SSF solar array temperatures; Albedo = 0.3, 56% Kapton bonded, 250 nm.

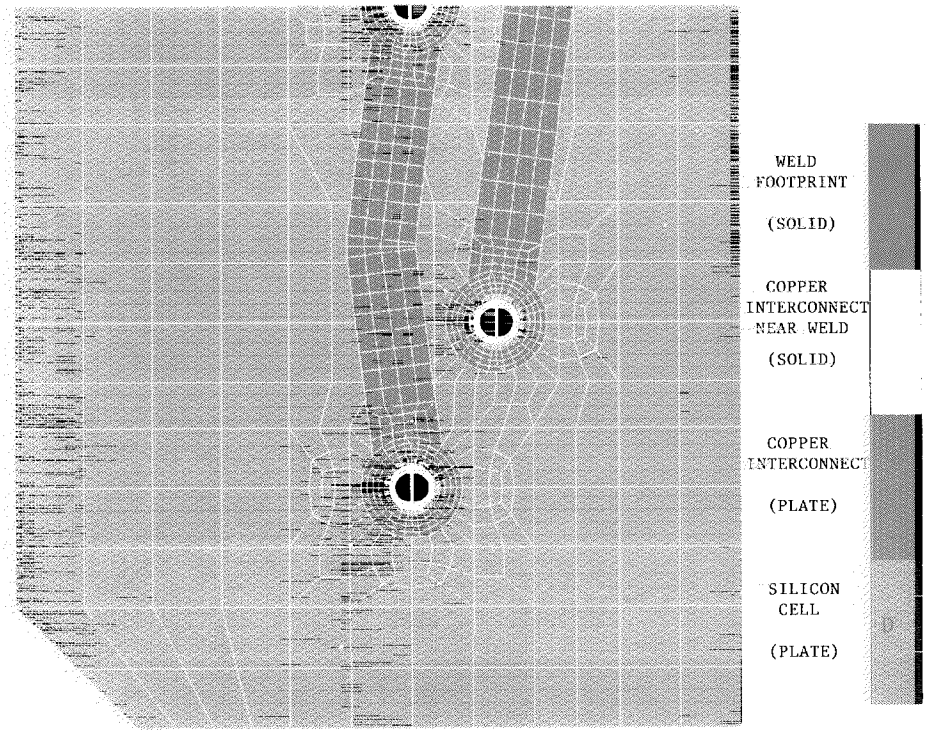

FIGURE 5: One Quarter Solar Cell Model

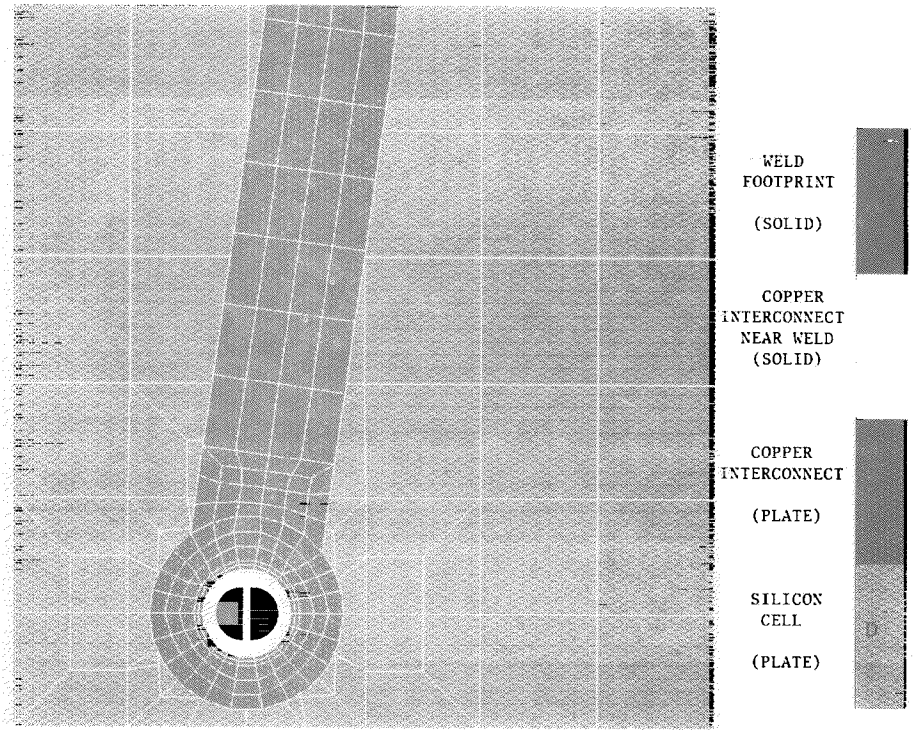

FIGURE 6: One-Half Copper Interconnector Model

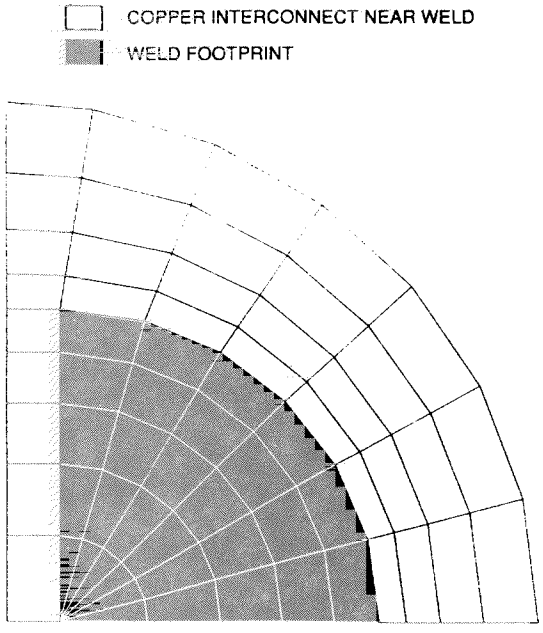

Figure 7. - One quarter weld area model.

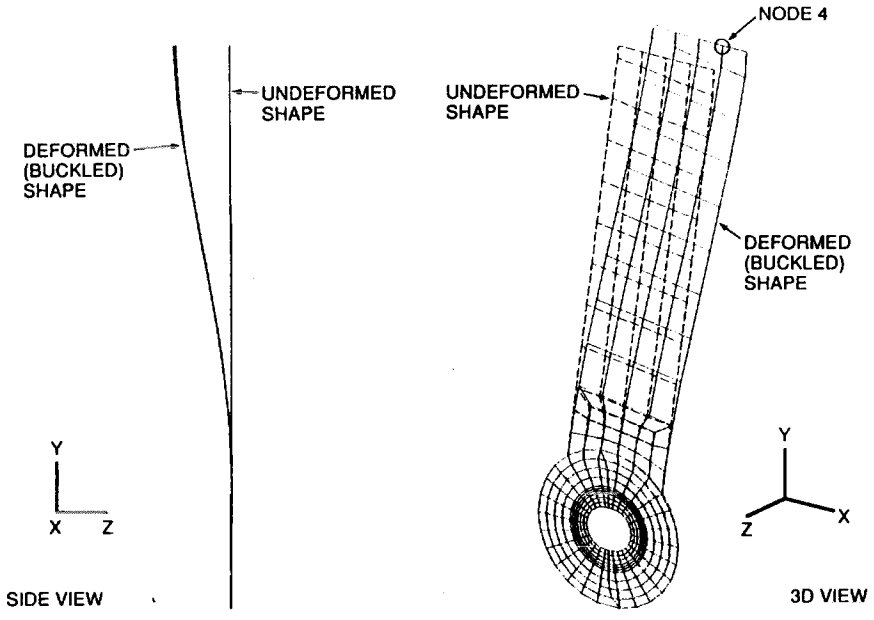

Figure 8. - First buckling mode of copper interconnector.

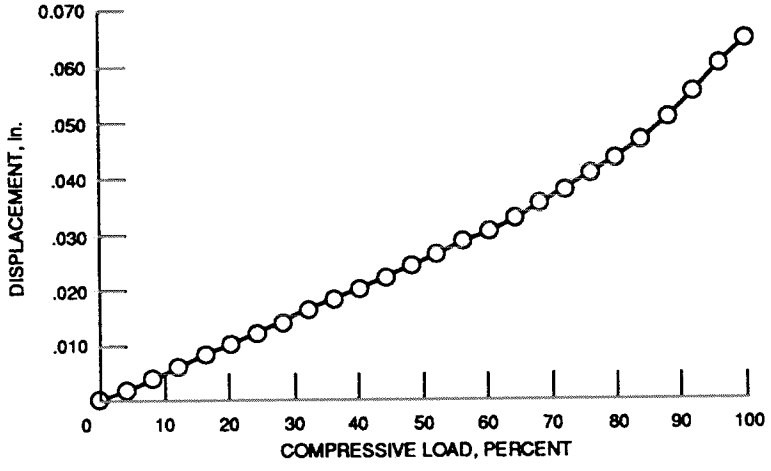

Figure 9. - Plot of Z-direction displacement of node 4 versus percentage of compressive load (see figure 8 for node 4).

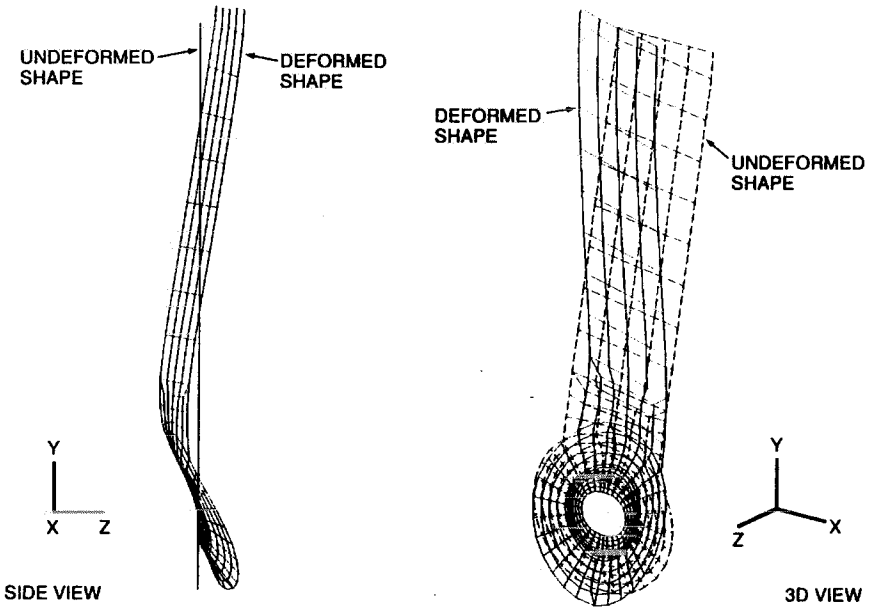

Figure 10. - Unloaded copper interconnector after plastic deformation.